Supporting Information for

Visualising diastereomeric interactions of chiral amine-chiral copper Salen adducts by EPR spectroscopy and DFT.

Damien M. Murphy,[1] Ignacio Caretti,[2] Emma Carter,[1] Ian A. Fallis,[1]

Marcus C. Göbel,[1] James Landon,[1] Sabine Van Doorslaer,[2] David J. Willock,[1]

[1]School of Chemistry, Cardiff University, Main Building, Park Place, Cardiff CF10 3AT, UK and [2]SIBAC laboratory – Department of Physics, University of Antwerp, Universiteitsplein 1, B-2610 Wilrijk, Belgium.

TABLE OF CONTENTS

(1) Further Experimental Details:

Preparation of samples for the EPR measurements

X-/Q-band CW-EPR/ENDOR*:* For CW-EPR/ENDOR measurements, a 1 ml volumetric stock solution of [Cu(**1,2**)] (0.100 g, 0.16 mmol) in dichloromethane was prepared and 200 μl (Hamilton glass microsyringes) aliquots of this solution were placed in 2 ml vials. The vials were placed in a heating block at 50°C and evaporated to dryness under a slow stream of nitrogen to afford [Cu(**1,2**)] as a purple glass. The vials were allowed to cool and to each 115 μl of dichloromethane and 115 μl of toluene was added to afford a high quality frozen solution. A number of additional EPR experiments were also performed (under similar conditions) using racemic (or enantiomeric *R*-, *S*-) methylbenzylamine (MBA). In the presence of amine, the parent complex was dissolved in 100 μl of dichloromethane and 100 μl of amine, with a small amount (30 μL) of toluene added to aid glass formation. The sample volume used in X-band EPR measurements was 150 μL, whereas 20 μL sample volume was used in Q-band ENDOR measurements.

W-band CW and pulsed EPR*:* First, a 32mM stock solution was prepared by dissolving the *R,R* or *S,S* form of the copper complex under study (Cu[**1**] or Cu[**2**]) in 1ml of dichloromethane. Then, 100μl aliquots of this solution were placed in 4ml vials and evaporated to dryness at 50°C under nitrogen atmosphere inside a glovebox. Finally, 230μl of toluene (in case of Cu[**1**]) or dichloromethane (in case of Cu[**2**]) was added to the vials. To study amine coordination, 200μl of either *R-,S-* or *rac*-methylbenzylamine (MBA) was added together with 30μl of toluene.

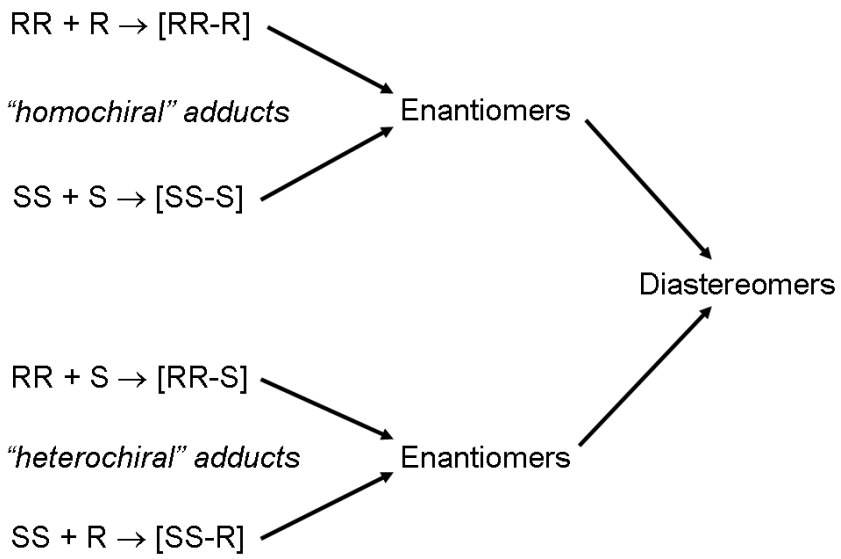

Scheme S1: Summary of the configurational stereoisomers examined: **RR** = *R,R*-[Cu(**1,2**)], **SS** = *S,S*-[Cu(**1,2**)], **R** = *R*-MBA, **S** = *S*-MBA. [**RR-R**] therefore represents the specific complex-amine adduct of *R,R*-[Cu(**1,2**)] + *R*-MBA.

(2) X-band EPR spectra of [Cu(2)] in MBA

Figure S1: X-band CW-EPR spectra recorded at 140K of (a) the non-coordinated [Cu(**2**)] complex in toluene:dichloromethane together with the different [Cu(**2**)]-MBA combinations of (b) *rac*-*rac*, (c) *RR*-*S*, (d) *SS*-*R*, (e) *RR*-*R* and (f) *SS*-*S*.

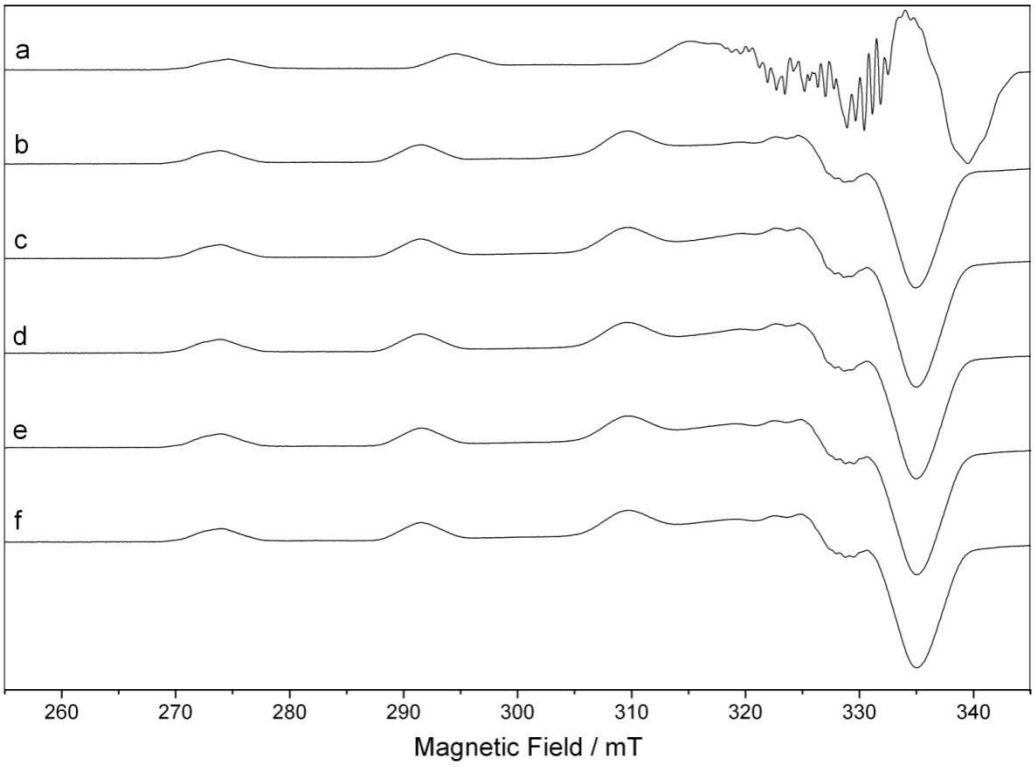

The equivalent series of spectra for [Cu(**1**)] were given in Fig.1 of main paper.

(3) Determination of the number of coordinated MBA molecules (*n*) to [Cu(1)]

A series of *rac-rac* samples, i.e., [Cu(**1**)]+MBA, were prepared using a constant concentration of [Cu(**1**)] (c = 3.3205 mmol dm^{-3}) and the ratio of MBA was varied from 1 to 20. The solvent used throughout was toluene. The resulting EPR spectra are shown in Fig.S2 below. For comparison, the EPR spectra of [Cu(**1**)] recorded in neat toluene (no amine; blue trace) and in an excess of amine (1:1200; red trace) are also shown.

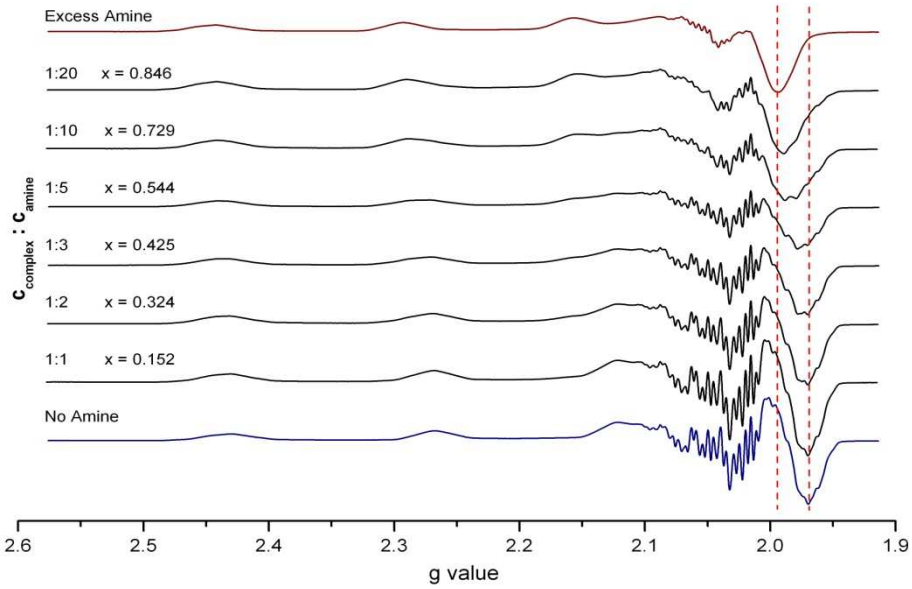

Figure S2: X-band CW-EPR spectra recorded at 130K of *rac*-[Cu(**1**)] dissolved in toluene with increasing concentrations of *rac*-MBA.

The spectra in Fig.S2 can be seen to progressively shift from the extreme cases of *no-amine present*, a typical non-coordinated spectrum (blue trace), to the *excess amine* case giving a coordinated spectrum (red trace). These shifts are most notable in the overshoot region of the spectra. The intervening EPR spectra (with Cu:MBA ratios ranging from 1:1 to 1:20) can then be treated as a linear combination of the blue and red base spectra. These intervening spectra were thus fitted using an algorithm based on combinations of red and blue spectra giving the coefficient *x* (the ratio of bound to unbound MBA): as expected *x* increases as the amount of MBA increases (Fig.S3). The data can then be analysed as follows to find *n* (the number of coordinated MBA's):

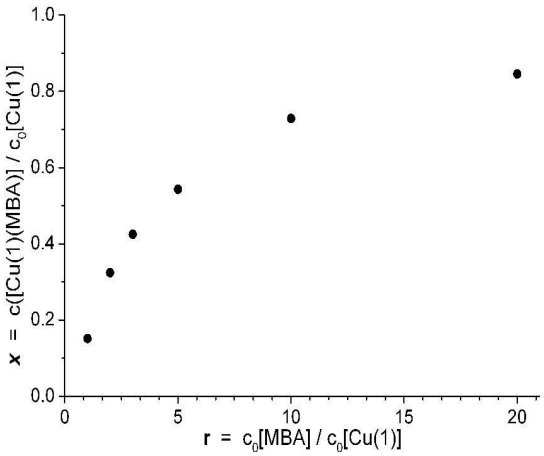

Figure S3: Effect of increasing MBA concentrations on the ratios *r* and *x*.

The equilibrium for MBA binding can be written as:

$$RR\text{-[Cu(ligand)]} + n\,R\text{-MBA} \leftrightarrow [\,RR\text{-Cu(ligand)}(R\text{-MBA})_n] \qquad \text{(eq.S1)}$$

$$K = \frac{c([Cu(ligand)(MBA)_n])}{c([Cu(ligand)]) \cdot c(MBA)^n} \quad \text{(eq.S2)}$$

Where *Cu(ligand)* represents either Cu(**1**) or Cu(**2**). If *r* represents the Cu:MBA ratio and c_0 the initial concentration, then:

$$c_0(MBA) = r \cdot c_0([Cu(ligand)]) \quad \text{(eq.S3)}$$

and

$$c([Cu(ligand)(MBA)_n]) = x \cdot c_0([Cu(ligand)]) \quad \text{(eq.S4)}$$

Therefore, the amount of non-coordinated MBA in the solution is given as:

$$\begin{aligned} c(MBA) &= c_0(MBA) - n \cdot c([Cu(ligand)(MBA)_n]) \\ c(MBA) &= r \cdot c_0([Cu(ligand)]) - n \cdot x \cdot c_0([Cu(ligand)]) \\ c(MBA) &= (r - n \cdot x) \cdot c_0([Cu(ligand)]) \end{aligned} \quad \text{(eq.S5)}$$

while the amount of non-coordinated Cu(ligand) is given as:

$$\begin{aligned} c([Cu(ligand)]) &= c_0([Cu(ligand)]) - c([Cu(ligand)(MBA)_n]) \\ c([Cu(ligand)]) &= (1 - x) \cdot c_0([Cu(ligand)]) \end{aligned} \quad \text{(eq.S6)}$$

Inserting eq.S5 and S6 into S2 gives:

$$K = \frac{x \cdot c_0([Cu(ligand)])}{(1-x) \cdot c_0([Cu(ligand)]) \cdot ((r - n \cdot x) \cdot c_0([Cu(ligand)]))^n} \quad \text{(eq.S7)}$$

$$K = \frac{x}{1-x} \cdot ((r - n \cdot x) \cdot c_0([Cu(ligand)]))^{-n} \quad \text{(eq.S8)}$$

$$\frac{x}{1-x} = K \cdot ((r - n \cdot x) \cdot c_0([Cu(ligand)]))^n \quad \text{(eq.S9)}$$

$$\begin{aligned} \ln\left(\frac{x}{1-x}\right) &= \ln(K) + n \cdot \ln(r - n \cdot x) + n \cdot \ln(c_0([Cu(ligand)])) \\ A &= \ln(K) + n \cdot \ln(c_0([Cu(ligand)])) \\ \ln\left(\frac{x}{1-x}\right) &= n \cdot \ln(r - n \cdot x) + A \end{aligned} \quad \text{(eq.S10)}$$

Since *r* ranges from 1 to 20 and is much larger than x (ranges from 0 to 1), the following simplification may be implemented:

$$\begin{aligned} & r >> x \\ & n \in \{1;2\} \\ & r - n \cdot x \approx r - x \end{aligned} \quad \text{(eq.S11)}$$

Hence:

$$\ln\left(\frac{x}{1-x}\right) \approx n \cdot \ln(r - x) + A \quad \text{(eq.S11)}$$

Thus a plot of ln(*x*/1-*x*) against ln(*r*-*x*) should give a straight line of slope *n*. The resulting graph is shown in Fig. S4 with $n = 1.04 \pm 0.15$.

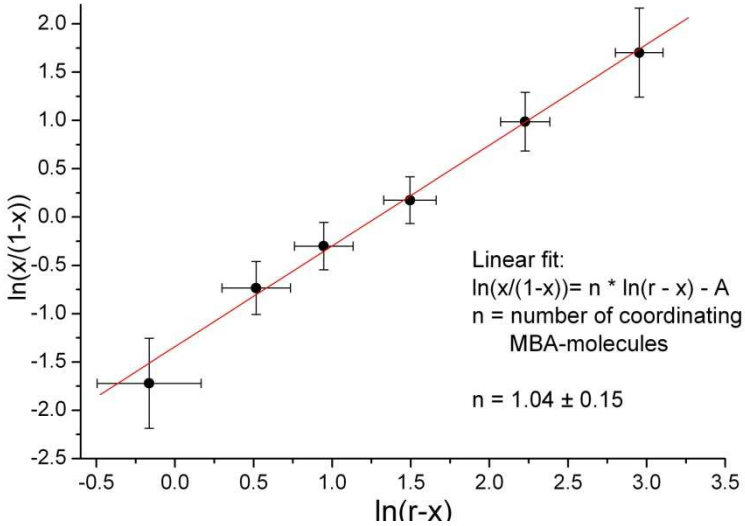

Figure S4: Plot of ln(*x*/1-*x*) against ln(*r*-*x*) for the determination of n, the number of coordinated MBA molecules in the [Cu(**1**)] complex.

Thus we can conclude that only 1 MBA molecule coordinates to [Cu(**1**)]. A similar treatment was also performed for [Cu(**2**)], where $n = 1$ was also found. These results are expected for such as bulky square planar Cu-salen complex interacting with a bulky MBA substrate.

(4) Supporting ^{1}H and ^{14}N ENDOR spectra

Figure S5; Q-band ^{1}H CW-ENDOR spectra (recorded at 10K) showing the H^{imine} couplings of (a) *rac*-[Cu(**1**)] dissolved in d^{8}-toluene/d^{6}-dichloromethane, and (b) *SS*-*R*, (c) *RR*-*S*, (d) *SS*-*S* and (e) *RR*-*R*. Spectra recorded at $g = g_{||}=g_3$ and $g = g_{\perp}=(g_1+g_2)/2$. For clarity, the central part of the spectra, containing proton couplings from the remaining ligand nuclei and coordinated MBA, have been removed.

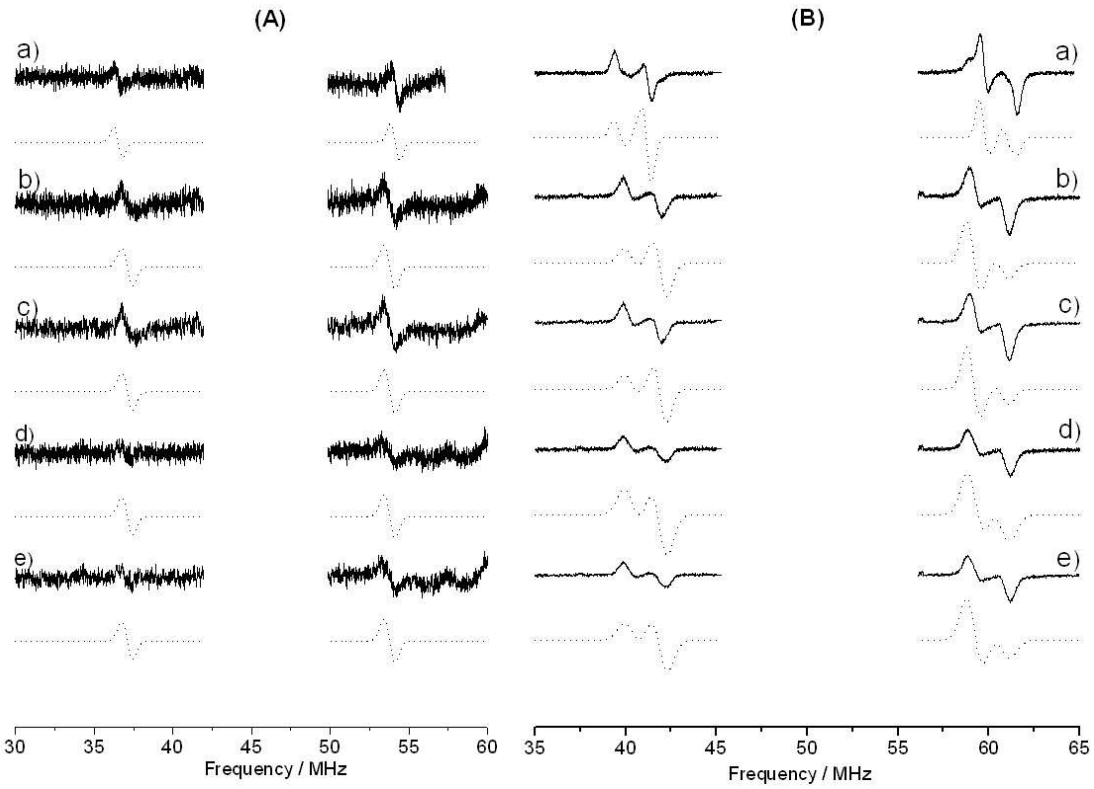

The equivalent series of spectra for the [Cu(**2**)] complex were given in Fig.4 of the main paper.

Table 1; ^{1}H principal hyperfine values for *R,R*-[Cu(**1**)] and *R,R*-[Cu(**2**)] dissolved in toluene/dichloromethane or MBA. For comparison the ENDOR data for the structurally related [Cu(Salen)] complex[42] is also shown.

Proton	A_1 / MHz	A_2 / MHz	A_3 / MHz	a_{iso} / MHz	[c]θ_H / °	$A_{dipolar}$ / MHz	R / Å	
Single Crystal[41]							ENDOR	X-ray
[a][Cu(Salen)] - H^{imine}	18.43 18.64	19.38 19.45	22.80 23.62	20.22 20.57	90		3.97 3.76	3.78 3.73
[a][Cu(Salen)] - $H^{methine}$	-1.43 -3.47	-1.43 -0.90	5.54 5.13	0.90 0.76	90		3.30 3.37	3.19 3.36
[b]tol/dcm								
[Cu(**1**)] - $H^{methine}$	-1.41	-1.43	5.54	0.91	50	4.63	3.30	
[Cu(**1**)] - $H^{tert\text{-}butyl}$	-1.64	-1.50	3.30	0.05	70	3.25	3.69	
[Cu(**1**)] - H^{imine}	18.5	17.2	22.1	19.27	90	2.83	3.84	
[Cu(**2**)] - H^{imine}	18.4	17.7	22.45	19.52	90	2.93	3.80	
[b]MBA								
[Cu(**1**)] - H^{imine}	17.2	16.6	21.0	18.26	90	2.73	3.90	
[Cu(**2**)] - H_a^{imine} - H_b^{imine}	16.6 16.6	17.2 16.1	21.3 21.3	18.37 18.00	90 90	2.93 3.30	3.81 3.66	
[Cu(**1**)] - H^{NH2}	-2.52	-4.87	3.62	-1.26	10	4.88	3.22	
[Cu(**2**)] - H^{NH2}	-2.62	-5.2	3.62	-1.40	10	5.02	3.18	

[a]Two crystallographically distinct sites identified in the single crystal ENDOR spectrum of [Cu(Salen)]. [b]The frozen solution ENDOR spectra of [Cu(**1,2**)] were recorded either using toluene/dicholomethane or neat MBA. [c]θ_H is defined as the angle between $\boldsymbol{g}_z$ and $\boldsymbol{A}_3$.

Figure S6; Q-band ^{1}H CW-ENDOR spectra (10K) of *rac*-[Cu(**1**)] dissolved in d^8-toluene/d^6-dichloromethane, recorded at (a) 1204.6, (b) 1197.7, (c) 1186.2, (d) 1165.7, (e) 1140.5, (f) 1117.7 and (g) 1086.8 mT. (experimental = solid, simulated = dashed line). Only the strongly coupled protons from the methine and *tert*-butyl groups are shown in the simulations (the remaining weak/remote ligand protons responsible for the inner intense peaks were not simulated, as the error in their assignment is significant). * = *tert*-butyl peak, ■ = methine peak.

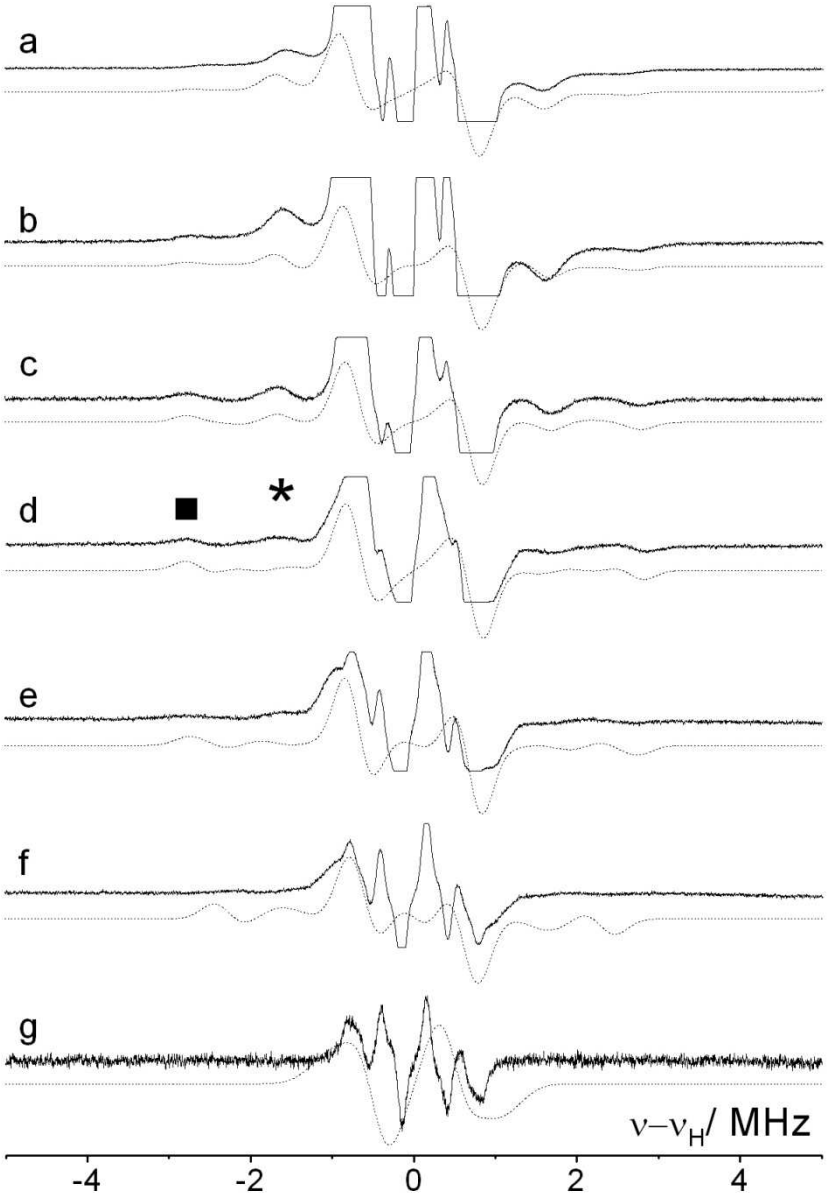

Figure S7; X-band ^{1}H CW-ENDOR spectra (10K) of (a) *rac*-[Cu(**1**)] and (b) *rac*-[Cu(**2**)] dissolved in d^8-toluene/d^6-dichloromethane, recorded at the field position corresponding to g = $g_{\|}$. The absence of the *tert*-butyl peak (*) in [Cu(**2**)] is very obvious compared to [Cu(**1**)]. The methine protons are present in both samples (■).

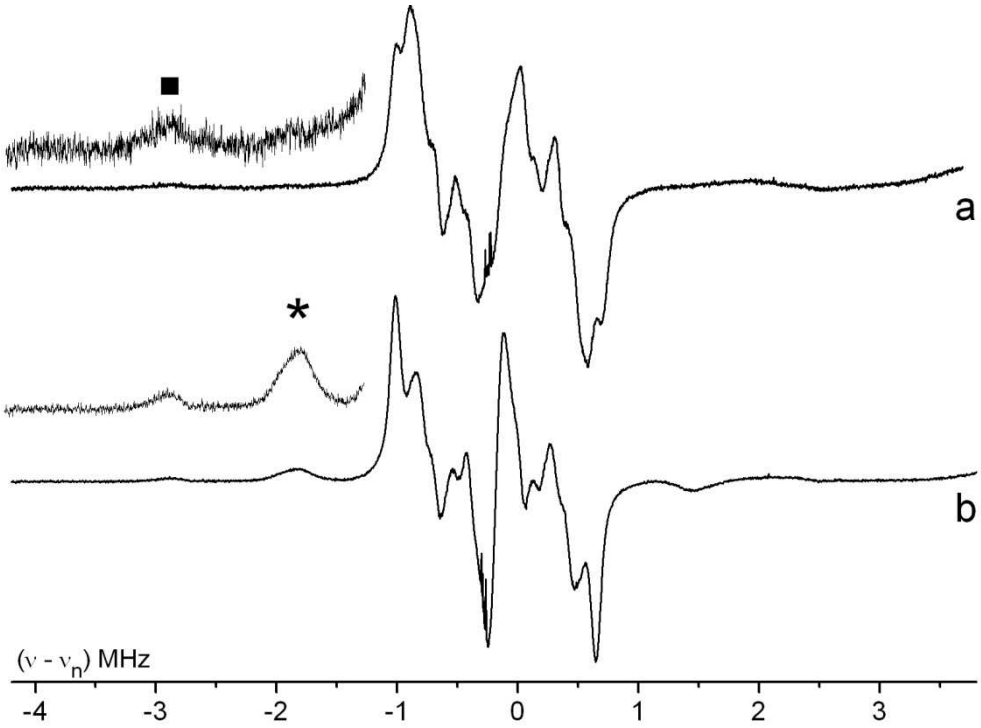

These spectra were used in the identification and assignment of the *tert*-butyl groups in [Cu(**1**)].

Figure S8: X-band Davies ENDOR spectra (recorded at 10K) of *rac*-[Cu(**1**)] dissolved in d^8-toluene/d^6-dichloromethane, recorded at the field positions (a) 340.0, (b) 333.0, (c) 327.0, (d) 320.6, (e) 310.0, (f) 300.0 and (g) 290.0 mT (experimental = solid, simulated = dashed line). Only the peaks for the methine and *tert*-butyl protons are included in the simulations.

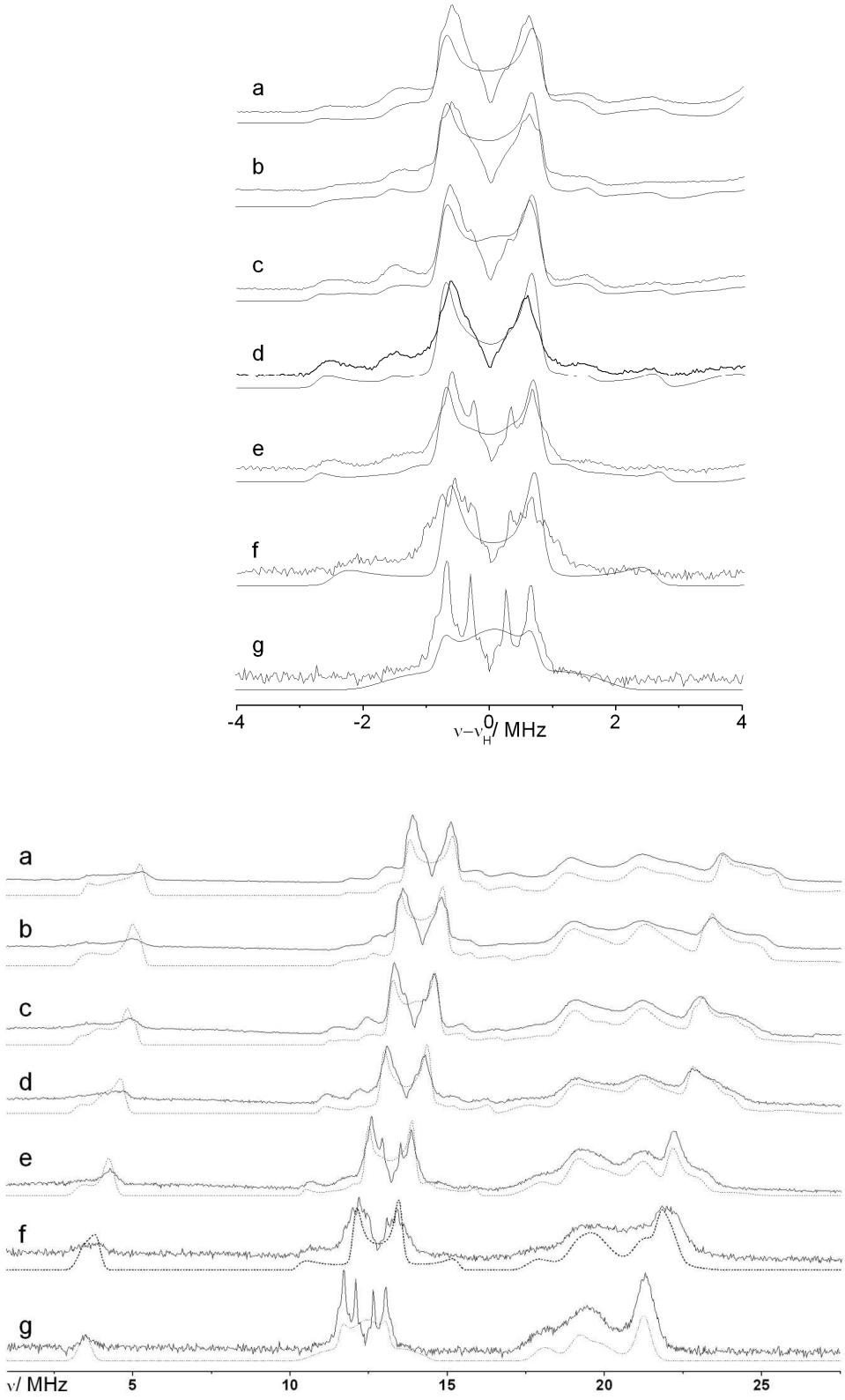

Figure S9: Q-band CW ^{1}H ENDOR spectra of *rac*-[Cu(**1**)] dissolved in *rac*-MBA recorded at the field positions of (a) 1191.0 (b) 1188.8 (c) 1171.7 (d) 1125.0 and (e) 1069.0 mT (experimental = solid, simulated = dashed line). The peaks labelled * are due to the ligand methine protons. Only the peaks for the amine protons are included in the simulations.

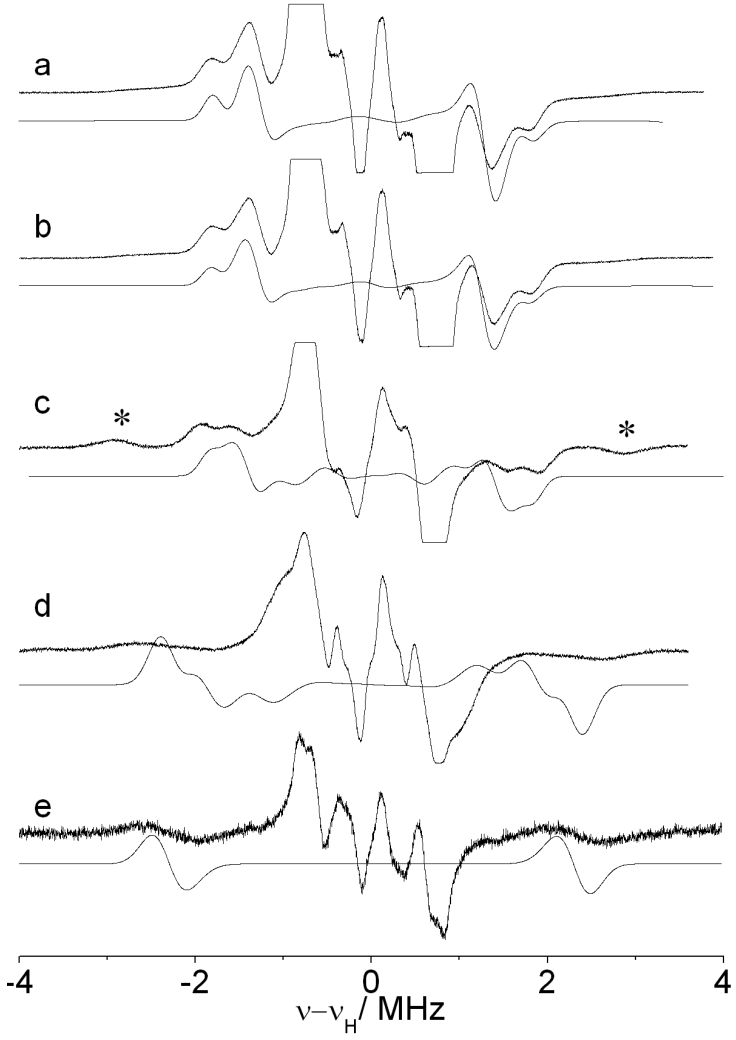

Figure S10; Q-band CW-^{1}H ENDOR spectra of *rac*-[Cu(**2**)] dissolved in *rac*-MBA recorded at (a) 1201.1, (b) 1191.9, (c) 1186.2, (d) 1142.8, (e) 1101.6 and (f) 1073.1 mT. (experimental = solid, simulated = dashed line).

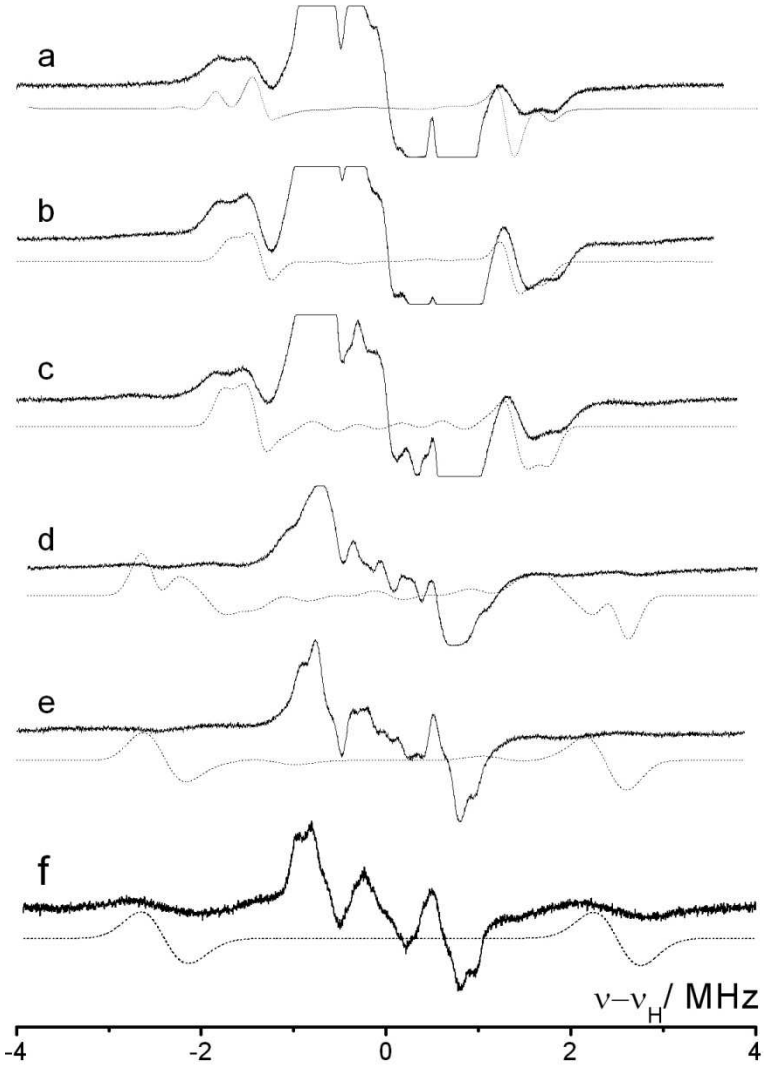

Figure S11; Q-band ^{1}H CW-ENDOR spectra (recorded at 10K) of *rac*-[Cu(**1**)] dissolved in d^8-toluene/d^6-dichloromethane, (b) *rac*-[Cu(**1**)] in *racemic* d^2-MBA, and (c) *rac*-[Cu(**1**)] in *rac*-MBA (protic). Spectra recorded at $g = g_{||}=g_3$ and $g = g_{\perp}=(g_1+g_2)/2$.

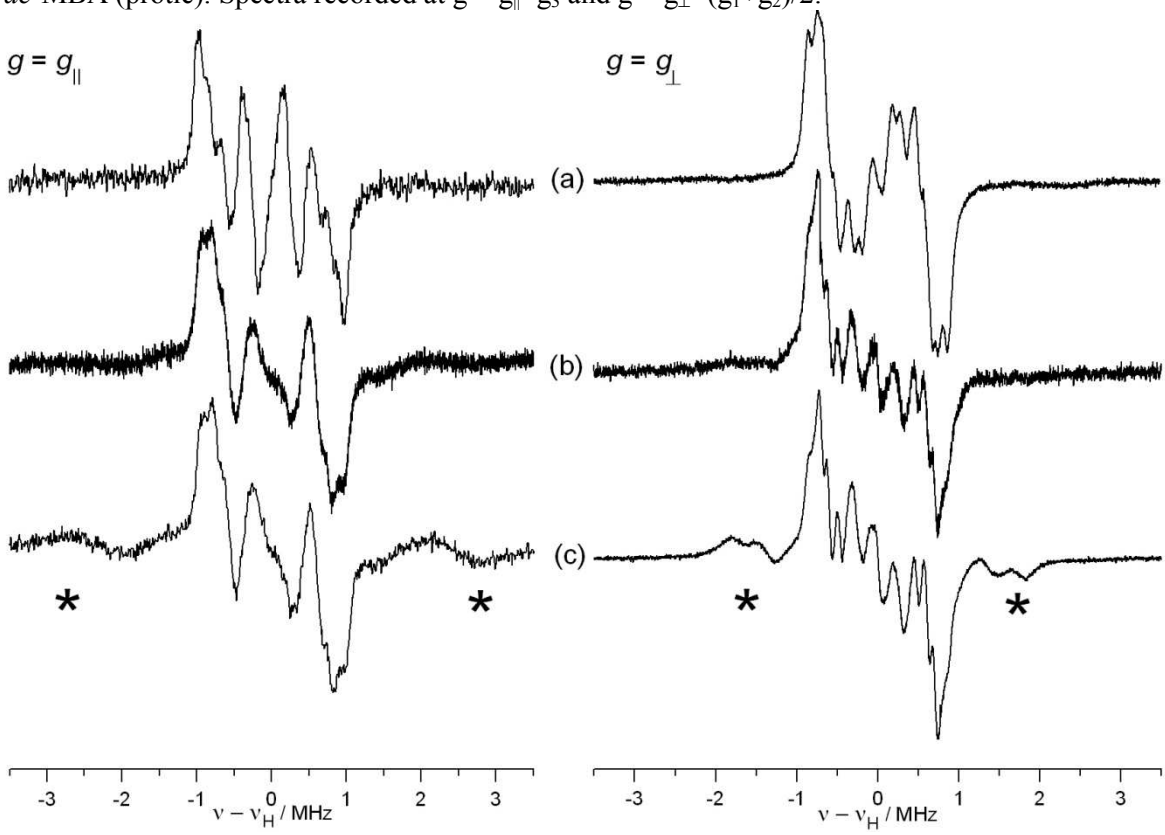

The $-NH_2$ protons from the coordinated MBA are labelled * in the Figure. These are clearly visible in (c), obtained using protic MBA, but largely absent in (b), recorded using d^2 deuterated-MBA. (Note; deuteration of MBA by D_2O does not give 100% exchange, hence the presence of residual MBA-NH_2 proton peaks in (b).

Figure S12; Q-band ^{14}N CW-ENDOR spectra of [Cu(**1**)] dissolved in (a,b) toluene and (c,d) MBA respectively. The spectra were recorded at the field positions (a,c) $g = g_{\perp}$ and (b,d) $g = g_{||}$. Solid lines = experimental, dashed lines = simulated.

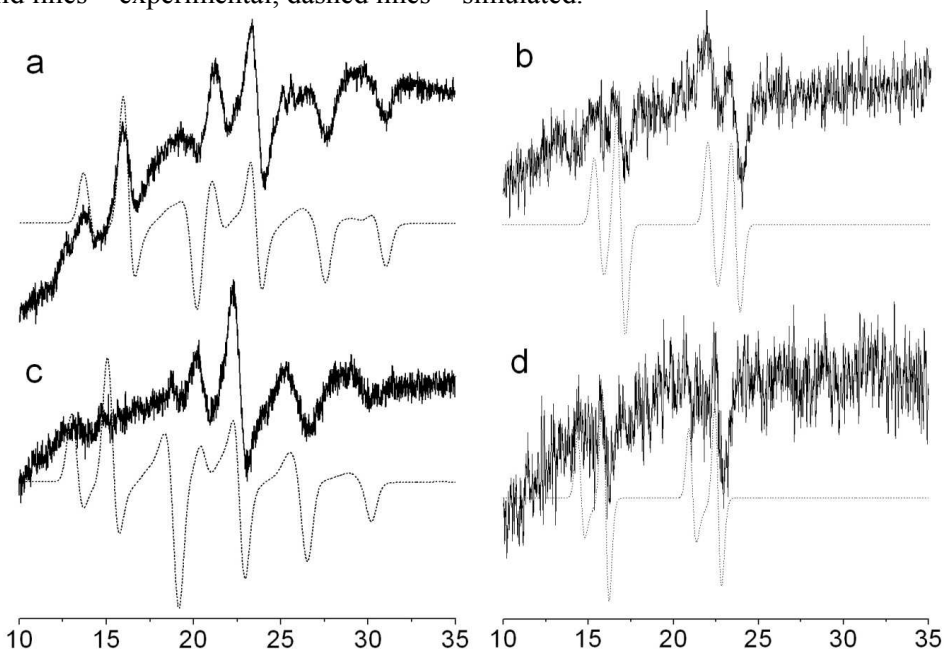

Figure S13: Q-band ^{14}N CW ENDOR spectra of [Cu(**2**)] dissolved in (a,b) toluene and (c,d) MBA respectively. The spectra were recorded at the field positions (a,c) $g = g_{\perp}$ and (b,d) $g = g_{||}$. Solid lines = experimental, dashed lines = simulated.

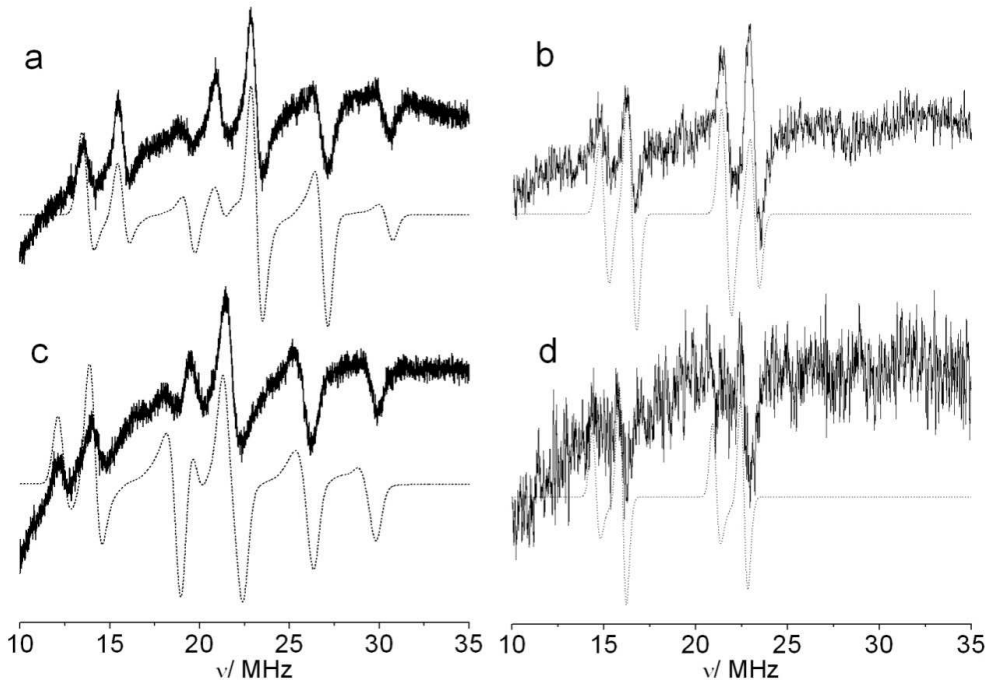

NOTE: simulations assuming the contributions of both nitrogen nuclei (with the hyperfine tensor in-plane rotated over 90^{o}) are identical to those assuming only one nitrogen, because of the near axiality of the ***g*** tensor.

(5) HYSCORE spectra

Figure S14: X-band HYSCORE spectra of *S,S*-[Cu(**1**)] dissolved in (a) toluene, (b) *R*-MBA and (c) pyridine, recorded at 15K around the $g = g_{\perp}$ field position (340 mT) with τ = 96ns and τ = 176 ns. (d) Simulation of spectrum (b) showing the weak interaction of the amine ^{14}N with [Cu(**1**)] (see text for parameters).

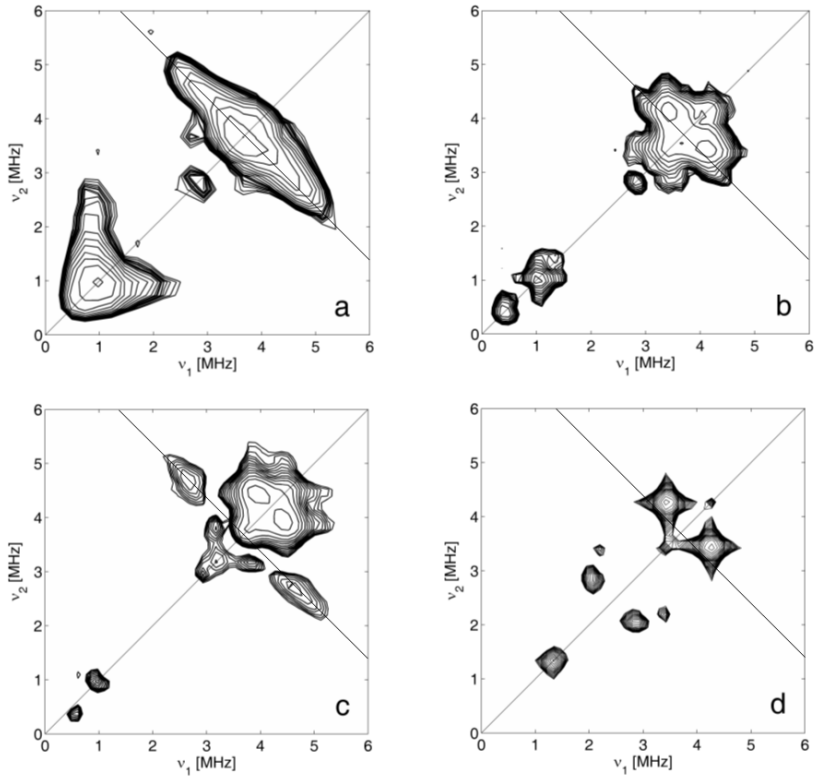

This Figure (a) shows the low-frequency region of the HYSCORE spectrum of [Cu(**1**)] in toluene, recorded at $g = g_{\perp}$. In the low-field area of the spectrum, a ridge due to interactions with the ^{13}C nuclei of ligand (**1**) is observed (^{13}C in natural abundance). The corresponding HYSCORE spectrum of [Cu(**1**)] in MBA is shown in (b). Two distinct peaks at ~(3.4, 4.2) MHz are observed, centred around the ^{13}C Larmor frequency and could thus stem from nearby ^{13}C nuclei in altered arrangement. However, in principle, an appropriate combination of ^{14}N hyperfine and nuclear quadrupole couplings could also lead to double-quantum cross-peaks at this position. To test this, the HYSCORE spectrum of [Cu(**1**)] dissolved in pyridine (Py) was recorded. The sp^2-hybridized nitrogen of pyridine is expected to have different nuclear quadrupole values compared to the sp^3-hybridized nitrogen of MBA. The resulting HYSCORE spectrum of [Cu(**1**)] in pyridine is given in (c). A clear shift of the double-quantum cross peaks, consistent with a larger nuclear quadrupole coupling of the ^{14}N nucleus, can be seen. The ^{13}C ridge found in (a) is now also visible, where earlier it was masked by the intense cross peaks in (b). The HYSCORE spectrum of [Cu(**1**)]+Py therefore proved that the cross peaks observed for [Cu(**1**)]+MBA are indeed due to the weak interaction with the amine nitrogen. The simulated parameters are given in Table 3.

(6) Additional DFT details

Figure S15: The starting model of [Cu(**1**)]+MBA used in QMMM calculations. *a*) Space fill atoms at QM level (BHandH), stick atoms at MM level (UFF). *b*) The torsion angle, φ, used to scan the orientation of MBA relative to the [Cu(**1**)] complex; this angle is defined with respect to **O**(Salen)···**Cu**···**N**(MBA···C*(MBA) where the defining atoms are shown as spheres in b).

Thus an angle of $\varphi = 0°$ is shown in b) where the C*(of MBA) atom is above the **O**(of Salen) atom. For clarity, the MBA-phenyl ring is shown oriented away from the complex. Clockwise turn is represented as –ve degrees and anticlockwise as +ve degrees.

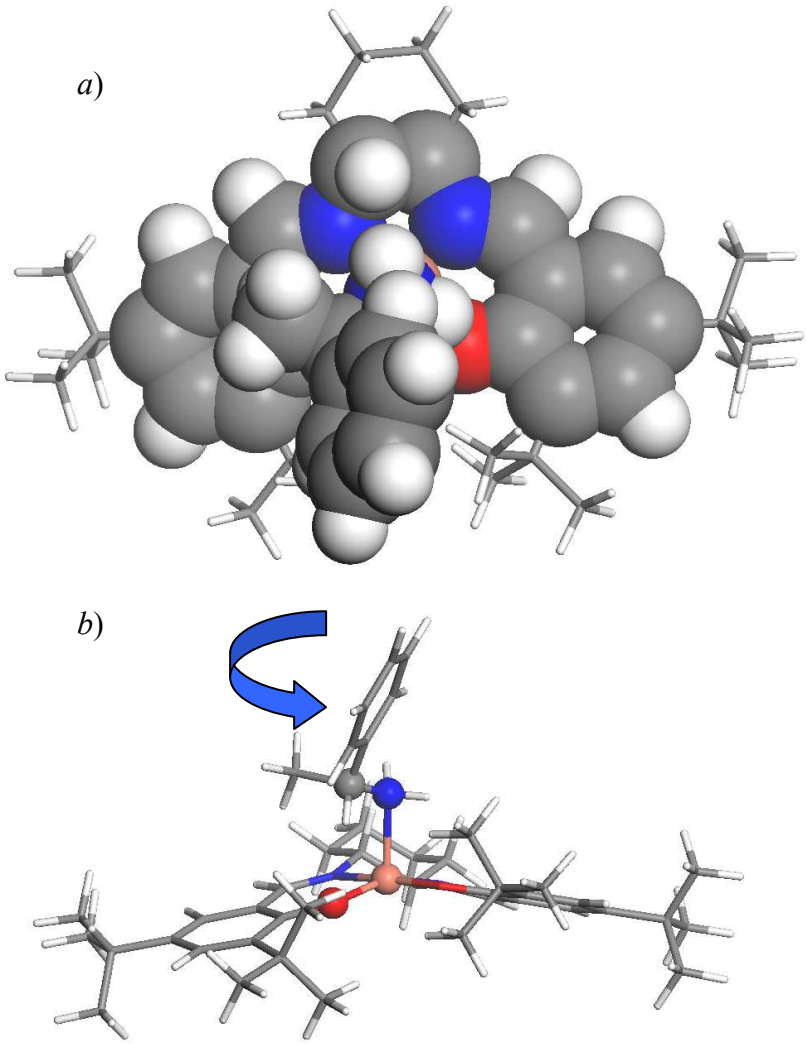

Figure S16: The relative energy *vs* torsion angle, φ (see Figure S15*b* for definition and value of $\varphi = 0°$) for *R*-MBA with *R,R*-[Cu(**1**)]. For this scan of the torsion angle Cu···N(MBA) is constrained to 2.2 Å and each point in the plot represents an optimisation with the additional constraint of torsion angle value. Structures from minima **A** and **B** were further optimised without constraints to produce the structures given in Figure 5 (main paper).

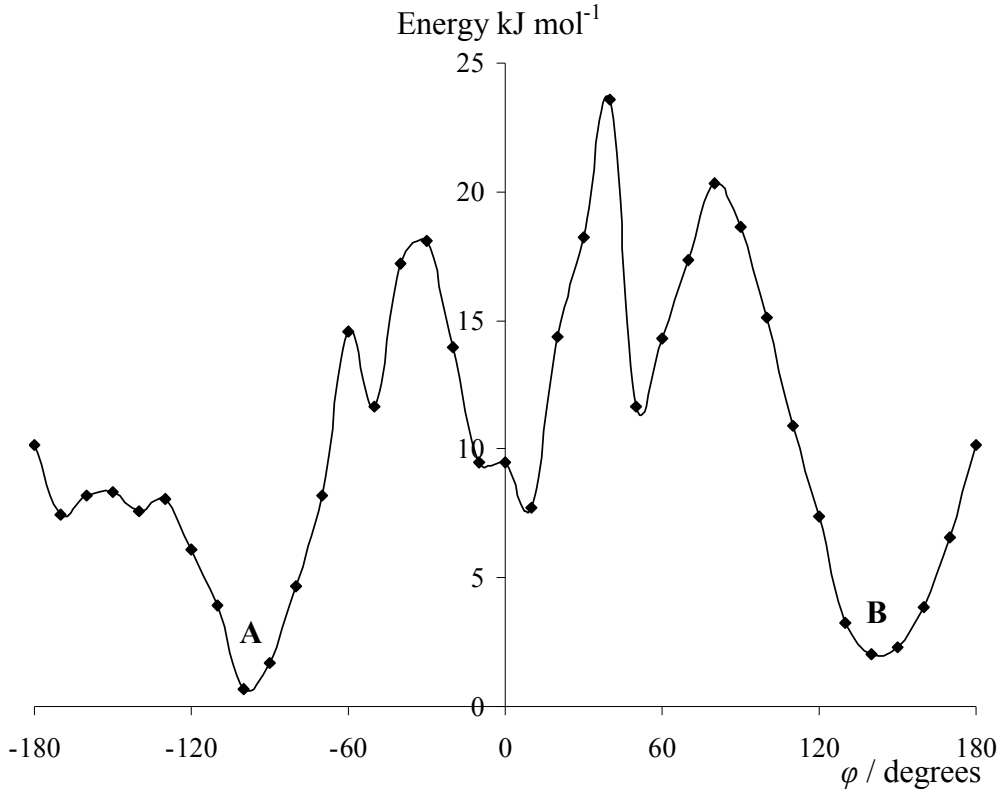

Full author details for reference (32) are:

[32] Gaussian 03, Revision C.02, Frisch, M.J.; Trucks, G.W.; Schlegel, H.B.; Scuseria, G.E.; Robb, M.A.; Cheeseman, J.R.; Montgomery, Jr. J.A.; Vreven, T.; Kudin, K.N.; Burant, J.C.; Millam, J.M.; Iyengar, S.S.; Tomasi, T.; Barone, V.; Mennucci, B.; Cossi, M.; Scalmani, G.; Rega, N.; Petersson, G.A.; Nakatsuji, H.; Hada, M.; Ehara, M.; Toyota, K.; Fukuda, R.; Hasegawa, J.; Ishida, M.; Nakajima, T.; Honda, T.; Kitao, O.; Nakai, H.; Klene, M.; Li, X.; Knox, J.E.; Hratchian, H.P.; Cross, J.B.; Bakken, V.; Adamo, C.; Jaramillo, J.; Gomperts, R.; Stratmann, R.E.; Yazyev, O.; Austin, A.J.; Cammi, R.; Pomelli, C.; Ochterski, J.W.; Ayala, P.Y.; Morokuma, K.; Koth, J.; Salvador, P.; Dannenberg, J.J.; Zakrzewski, V.G.; Dapprich, S.; Daniels, A.D.; Strain, M.C.; Farkas, O.; Malick, D.K.; Rabuck, A.D.; Raghavachari, K.; Foresman, J.B.; Ortiz, J.V.; Cui, Q.; Baboul, A.G.; Clifford, S.; Cioslowski, J.; Stefanov, B.B.; Liu, G.; Liashenko, A.; Piskorz, P.; Komaromi, I.; Martin, R.L.; Fox, D.J.; Keith, T.; Al-Laham, M.A.; Peng, C.Y.; Nanayakkara, A.; Hallacombe, M.; Gill, P.M.W.; Johnson, B.; Chen, W.; Wong, M.W.; Gonzalez, C. and Pople, J.A.; Gaussian, Inc., Wallingford CT, **2004**.